https://doi.org/10.5194/tc-2022-132
Preprint. Discussion started: 26 July 2022

The Cryosphere Discussions

Ice thickness and water level estimation for ice-covered lakes with satellite altimetry waveforms and backscattering coefficients

Xingdong Li[1, 3], Di Long[1, 3], Yanhong Cui[1, 3], Tingxi Liu[2, 3], Jing Lu[4], Mohamed A. Hamouda[5, 6], and Mohamed M. Mohamed[5, 6]

[1]State Key Laboratory of Hydroscience and Engineering, Department of Hydraulic Engineering, Tsinghua University, Beijing 100084, China
[2]Water Conservancy and Civil Engineering College, Inner Mongolia Key Laboratory of Water Resource Protection and Utilization, Inner Mongolia Agricultural University, Hohhot, 010018, China
[3]Collaborative Innovation Center for Integrated Management of Water Resources and Water Environment in the Inner Mongolia Reaches of the Yellow River, Hohhot, 010018, China
[4]State Key Laboratory of Remote Sensing Science, Aerospace Information Research Institute, Chinese Academy of Sciences, Beijing 100101, China
[5]Department of Civil and Environmental Engineering, United Arab Emirates University, Al Ain, 15551, United Arab Emirates
[6]National Water and Energy Center, United Arab Emirates University, Al Ain, 15551, United Arab Emirates

Correspondence to: Di Long (dlong@tsinghua.edu.cn) and Tingxi Liu (txliu1966@163.com)

Abstract. Lake ice, serving as a sensitive indicator of climate change, is an important regulator of regional hydroclimate and lake ecosystems. For ice-covered lakes, traditional satellite altimetry-based water level estimation is often subject to winter anomalies that are closely related to the thickening of lake ice. Despite recent efforts made in exploiting altimetry data to resolve the two interrelated variables, i.e., lake ice thickness (LIT) and water level of ice-covered lakes, several important issues remain unsolved, including the inability of estimating LIT with altimetric backscattering coefficients in ungauged lakes due to the dependence on in situ LIT data. It is still unclear what role lake surface snow plays in the retrieval of LIT and water levels in ice-covered lakes with altimetry data. Here we developed a novel method to estimate lake ice thickness by combining altimetric waveforms and backscattering coefficients without using in situ LIT data. To overcome complicated initial LIT conditions and better represent thick ice conditions, a logarithmic regression model was developed to transform backscattering coefficients into LIT. We investigated differential impact of lake surface snow on estimating water levels for ice-covered lakes when different threshold retracking methods are used. The developed LIT estimation method, validated against in situ data and cross-validated against modelled LIT shows an accuracy of ~0.2 m and is effective in detecting thin ice that cannot be retrieved by altimetric waveforms. We also improved estimation of water levels for ice-covered lakes with a strategy of merging lake water levels derived from different threshold methods. This study facilitates a better interpretation of satellite altimetry signals from ice-covered lakes and provides opportunities for a wider application of altimetry data to the cryosphere.

https://doi.org/10.5194/tc-2022-132
Preprint. Discussion started: 26 July 2022

1 Introduction

Lake ice plays a unique and critical role in regulating lake ecosystems through the modulation of fluxes in and out of the lake, e.g., solar radiation, evaporation, sensible heat, and methane emission (Cooley et al., 2020; Engram et al., 2020; Sharma et al., 2019; Wang et al., 2018; Wik et al., 2016; Woolway et al., 2020). The vulnerability of lake ice to climate change causes wide concern to the stability of boreal lake ecosystems and the sustainability of socioeconomic activities that rely on lake ice (Knoll et al., 2019; Mullan et al., 2017). Lake ice cover and LIT are two Essential Climate Variables (ECVs) related to lake ice identified by the Global Climate Observing System (GCOS). Lake ice cover is a measure of lake ice quantity (horizontally). LIT can provide information on both lake ice quantity (vertically) and quality (e.g., the strength of lake ice), which is highly related to the safety of human activities on ice. For instance, LIT loss could reduce the availability of ice roads (Li et al., 2022) and increase the possibility of winter drowning (Sharma et al., 2020). However, compared with the intensively investigated lake/river ice cover (Du et al., 2017; Yang et al., 2020; Kropácek et al., 2013), the knowledge of LIT is largely limited, due mostly to the lack of in situ observations and effective remote sensing-based methods. There is a considerable gap between the monitoring accuracy of LIT expected by the GCOS (1–2 cm) and that of current remote sensing-based approaches (0.1–0.2 m). For winter water level estimation based on altimeters, the existence of lake ice is a barrier that could cause an abrupt decrease in altimetric lake surface height (LSH) (Shu et al., 2020). To resolve this issue, a better understanding of the impact of lake ice and lake surface snow on altimetric signals is necessary.

Current remote sensing of LIT is based mostly on information from thermal infrared sensors and microwave sensors (Murfitt and Duguay, 2021). Thermal infrared information such as lake surface temperatures can be used to drive a freezing degree day-based model or more sophisticated lake ice models to estimate LIT (Yu and Rothrock, 1996; Zeng et al., 2016; Li et al., 2022). However, cloud contamination and complex physical processes related to lake surface snow (Cheng et al., 2013; Duguay et al., 2003) could limit the accuracy and robustness of the method based on thermal infrared information and lake ice modelling. Microwave information has a certain penetration depth (Atwood et al., 2015) within the lake ice and is not affected by cloud cover, providing great potential of more direct and robust observations of LIT.

Some previous studies focused on the use of passive microwave information, i.e., brightness temperature (T_B) obtained by satellite radiometers. Kang et al. (2010) explored the relationship between T_B obtained by AMSR-E and LIT in two Canadian lakes, Great Slave Lake (GSL) and Great Bear Lake (GBL), indicating that the increase in LIT is associated with the increase in T_B. They later showed that, with a linear regression model, an 18.7 GHz T_B could best represent the LIT accumulation and the accuracy (root mean squared error, RMSE) was ~0.18 m (Kang et al., 2014). Passive microwave methods perform well in terms of high temporal resolution (daily) but are limited to a few large lakes due to the low spatial resolution, as the pixel size of the 18.7 GHz T_B is 25 km.

Active microwave remote sensing of LIT can be further categorized into classes based on: (1) backscattering coefficients or (2) satellite altimetry waveforms. As for backscattering coefficients, those derived from SAR images and those from satellite

https://doi.org/10.5194/tc-2022-132
Preprint. Discussion started: 26 July 2022

altimeters have very different behaviours during ice seasons. Backscattering coefficients of SAR images would experience a rapid decrease when the lake surface is covered by skim ice (a quasi-specular reflector), followed by a steady increase with the accumulation of LIT until the floating lake ice becomes bedfast lake ice or the melting starts (Duguay and Lafleur, 2003; Murfitt and Duguay, 2021; Howell et al., 2009; Murfitt et al., 2018). On the contrary, backscattering coefficients from satellite altimeters would experience a rapid increase when the open water is covered with skim ice, followed by a steady decrease with the thickening of LIT until the melting starts. Given the mentioned behaviours, backscattering coefficients from SAR images were widely used in discriminating bedfast lake ice from floating lake ice and monitoring of lake/sea ice phenology (Howell et al., 2018; Howell et al., 2019). Backscattering coefficients from satellite altimeters were also used in lake ice phenology. A recent study (Zakharova et al., 2021) investigated the relationship between the altimetry-based backscattering coefficients and in situ river ice thickness, suggesting the great potential of altimetry-based backscattering coefficients in estimating LIT for thin ice. However, in situ ice thickness data are necessary to derive regression models, which greatly limits applications of the method developed by Zakharova et al. (2021). To avoid confusion, the term "backscattering coefficients" refers to altimetry-based backscattering coefficients in the following context, unless otherwise stated.

LIT estimation based on satellite altimetric waveforms was first investigated by Beckers et al. (2017) with double-peak waveforms from CryoSat-2 on GSL and GBL, which provides a potential approach for robust LIT monitoring because the method is physically-based and does not rely on parameterization. Shu et al. (2020) combined the method developed by Beckers et al. (2017) in winter water level retrieval using Sentinel-3 data. CryoSat-2 and Sentinel-3 are SAR altimeters with pulse-doppler-limited footprints, which can be regarded as beam-limited footprints. Compared with traditional pulse-limited altimeters such as TOPEX/Poseidon (T/P) and Jason-1/2/3 (available since 1992), the time span of SAR altimeters such as CryoSat-2 and Sentinel-3 is relatively short (i.e., CryoSat-2 was launched in 2010 and Sentinel-3A was launched in 2016). The method developed by Beckers et al. (2017) is not that compatible with traditional pulse-limited altimeters, because the waveforms of pulse-limited altimeters are largely different from those from SAR altimeters. Li et al. (2022) developed a LIT estimation method suitable for pulse-limited altimeters T/P and Jason-1/2/3. Therefore, the time span of retrievable LIT has been increased substantially from ~10 years to almost three decades. The temporal resolution has also been largely improved because T/P and Jason-1/2/3 have the shortest revisit cycle (~10 days) among all existing satellite altimeters. However, the LIT estimation for thin ice based on radar waveforms is limited by the range resolution of the waveform. For instance, the minimum LIT retrievable with the method developed by Beckers et al. (2017) is 0.263 m for CryoSat-2 theoretically. For Jason-1/2/3, Li et al. (2022) suggested that the LIT retrieval is robust after LIT exceeds 0.4 m because the waveforms of Jason-1/2/3 have a coarser range resolution than CryoSat-2.

Water level estimation for ice-covered lakes has been investigated with different approaches for different altimeters (Shu et al., 2020; Yang et al., 2021; Ziyad et al., 2020). Ziyad et al. (2020) developed a classification scheme to separate Jason-2 observations from the ice-covered lake surface from the open water surface, and only used open water observations to derive water level time series to avoid the contamination from lake ice. Shu et al. (2020) applied the method developed by Beckers

https://doi.org/10.5194/tc-2022-132
Preprint. Discussion started: 26 July 2022

et al. (2017) to estimate LIT using Sentinel-3, and then derived a range correction associated with LIT to correct the abrupt drop in winter altimetric water levels. Yang et al. (2021) tested several threshold retracking algorithms to develop a modified subwaveform threshold (MST) retracking method for two-peak waveforms from T/P and Jason-1/2/3 to improve water level estimation during ice seasons. The MST retracking algorithm could avoid winter water level anomalies for most cases and the metrics of derived altimetric water levels are quite promising, e.g., the standard deviations (STDs) of the differences between altimetric water levels and in situ water levels are mostly smaller than 0.1 m among study lakes (GSL, GBL, and Athabasca Lake). However, an important issue remains to be further discussed. Causes of the two-peak waveforms are still not clear and could be attributed to multiple backscattering surfaces, i.e., snow surface, snow-ice interface, and ice-water interface. Yang et al. (2021) suggested that the first subwaveform of Jason-1/2/3 waveforms from ice-covered lake surfaces corresponds to snow-ice interfaces based on the comparison with in situ water levels. However, Li et al. (2022) suggested that the first subwaveform corresponds to the snow surface for most Canadian lakes based on the comparison with in situ ice and snow thickness. Better understanding the paradox of the forming of altimetry radar waveforms from ice-covered lake surfaces could benefit the retrieval of winter water levels as well as LIT.

This study was designed to: (1) combine satellite altimetry-based waveforms and backscattering coefficients to improve LIT estimation for ungauged lakes and thin ice, and (2) explore possible improvements in altimetric water level estimation for ice-covered lakes through a better understanding of altimetric signals from snow and ice-covered lake surfaces. As mentioned above, LIT estimation based on waveforms alone is ineffective for thin ice and altimetry-based backscattering coefficients have the potential to monitor thin ice. Meanwhile, the dependence on in situ data limits a wider application of altimetry-based backscattering coefficients to LIT estimation. Therefore, the combination of these two methods (satellite altimetry-based backscattering coefficients and waveforms) could be complementary. To exploit the potential of backscattering coefficients in LIT estimation, we derived a logarithmic regression model to better represent various lake ice conditions, which is detailed in Sect. 3.2 and Sect. 4.1. As for water level estimation, we mainly explored different behaviours of lake surface snow when different threshold methods were used. We then developed an approach of merging water level time series derived from different threshold methods.

This paper is organized as follows. Sect. 2 introduces the study area and data used. Sect. 3 provides details on LIT estimation based on the combination of backscattering coefficients and waveforms from satellite altimetry, as well as a novel water level estimation method for ice covered lakes. Sect. 3 also includes a detailed deduction of a novel logarithmic regression model used to convert backscattering coefficients into LIT. Sect. 4 shows the performance of the logarithmic model and the validation of LIT and water level estimation methods. Sect. 5 discusses differential impact of lake surface snow when different threshold methods are used, uncertainty sources of LIT estimation and water level retrieval, and implications of this study in future lake ice and lake water level research. Sect. 6 summarizes the main findings of this study.

https://doi.org/10.5194/tc-2022-132
Preprint. Discussion started: 26 July 2022

2 Study area and data

2.1 Study area

As shown in Fig 1, we investigated seven lakes, including five lakes in Canada, i.e., GBL (121.30°W, 65.91°N), GSL (114.37°W, 62.09°N), Athabasca Lake (109.96°W, 59.10°N), Winnipeg Lake (97.25°W, 52.12°N), and Baker Lake (95.28°W, 64.13°N), and two lakes in Asia, i.e., Hulun Lake (117.38°E, 48.97°N) and Har Lake (93.21°E, 48.05°N). GBL, GSL, and Athabasca Lake are located in the Mackenzie River basin, where annual precipitation ranges between 300 mm and 1,000 mm from northeast to southwest. Typical mean monthly temperatures of the Mackenzie River basin range from -35°C to -25°C in winter and from 15°C to 20°C in summer (Howell et al., 2009). Baker Lake is located in the northeast part of Canada, with a mean July air temperature of 11.4°C and a mean annual precipitation of 157 mm (Medeiros et al., 2012). Winnipeg Lake covers a wide range of latitudes and mean annual air temperatures vary considerably from south (1.6°C) to north (-0.7°C). Mean annual precipitation in the Winnipeg Lake basin is 498 mm (Stewardship, 2011). Hulun Lake has a mean annual temperature of ~0°C and most of precipitation takes place from June to September due to a continental monsoon climate (Cai et al., 2016). Har Lake (Khar Lake) is located in a desert in Mongolia, with annual precipitation that is likely less than 100 mm. LIT in GSL, Baker Lake, Hulun Lake, and Har Lake was derived from altimetry data and compared with either in situ data or model simulations. LSH in GBL, GSL, Athabasca Lake, and Winnipeg Lake was derived from altimetry data and validated with in situ water levels.

https://doi.org/10.5194/tc-2022-132
Preprint. Discussion started: 26 July 2022

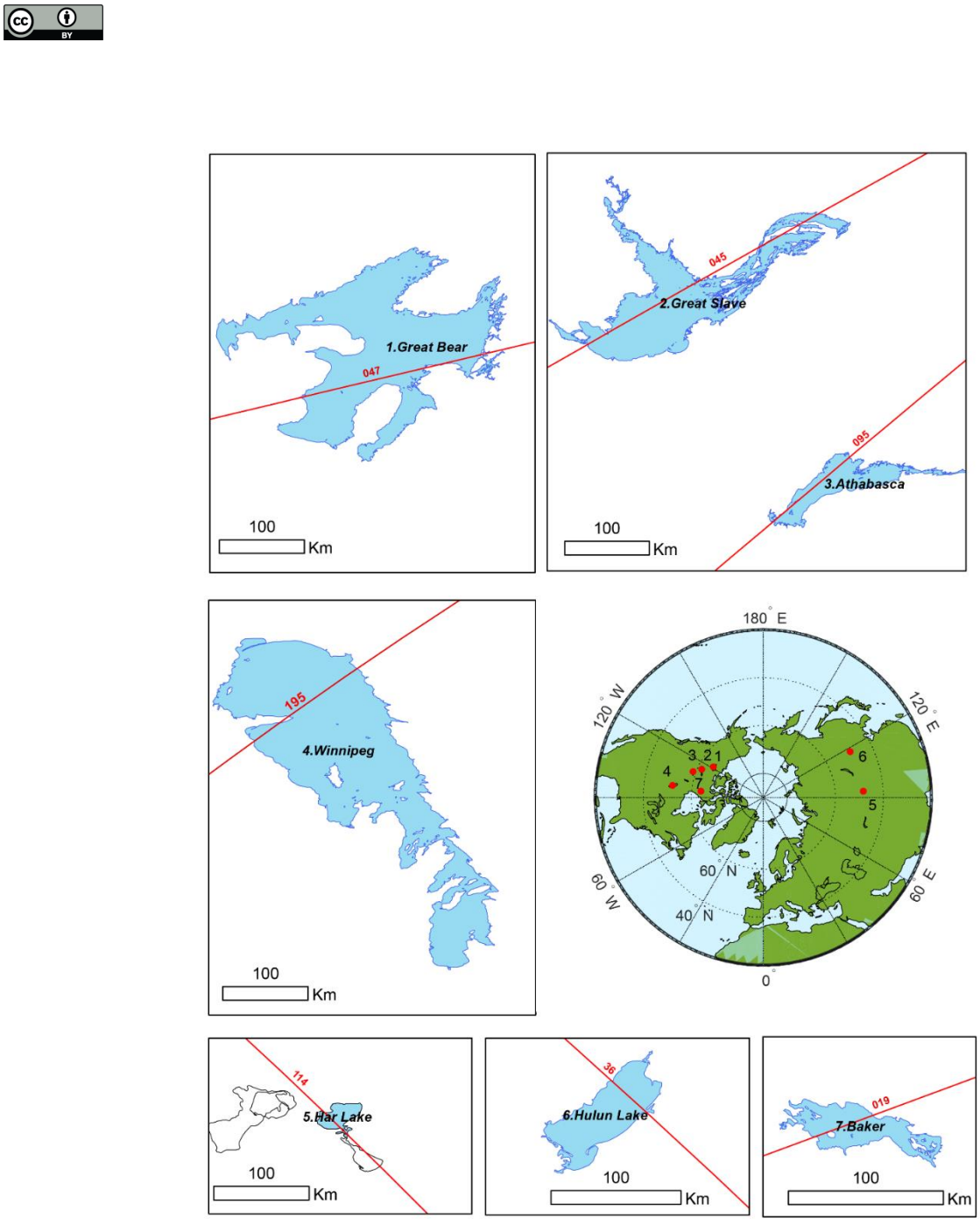

Figure 1: Study lakes and satellite altimetry ground tracks used. Red curves denote ground tracks of T/P and Jason-1/2/3.

145

2.2 Data

Satellite altimeters were initially designed for monitoring ocean topography and ice sheets. Nevertheless, numerous studies have explored the potential of satellite altimetry in monitoring inland waters such as river water levels and discharge, lake

https://doi.org/10.5194/tc-2022-132
Preprint. Discussion started: 26 July 2022

water levels and storage changes, glacier elevation changes and mass balance, and recently in LIT (Huang et al., 2019; Zhang et al., 2021; Zhao et al., 2022; Li et al., 2022; Huang et al., 2018; Li et al., 2019). Satellite altimetry data we used here were collected by Jason-1/2/3, covering the 2002–2020 period. Ground tracks for each lake are shown in Fig. 1. Jason-1/2/3 are follow-on missions of T/P and inherited the orbit of their predecessor. T/P and Jason-1/2/3 have the shortest revisit time of ~10 days among existing satellite altimetry missions, providing observations from 66 °N to 66 °S. Radar altimeters carried by Jason-1/2/3 are dual-frequency (Ku-band and C-band) pulse-limited altimeters. Pulse-limited essentially means that the size of radar altimetry illuminated area/footprints is limited by the pulse width, as opposed to the beam width (such as laser altimeters and SAR altimeters). As a result, the trailing edge of pulse-limited waveforms is milder and noisier than that of beam-limited waveforms, adding to the difficulty of retrieving LIT based on waveforms.

Altimetry products used here were the Sensor Geophysical Data Records (SGDR), containing waveforms, backscattering coefficients for Ku-band and C-band, satellite altitude, uncorrected range, and range corrections (atmospheric corrections and geophysical corrections) for 20 Hz footprints (20 footprints per second, with a spacing of ~330 m). The SGDR products also contain corrected ranges using default retracking algorithms (MLE3 and MLE4), but have been shown unreliable in water level estimation for ice-covered lakes (Yang et al., 2021). However, it does not mean that default retracking algorithms (MLE3 and MLE4) are irrelevant to this study. On the contrary, backscattering coefficients provided in the SGDR products are generated from the MLE4 retracking algorithm and are highly related to the amplitude of the waveforms. The altimetry data used can be obtained from the Archiving, Validation, and Interpretation of Satellite Oceanographic (AVISO+) (http://ftp-access.aviso.altimetry.fr).

To validate the derived LIT, we obtained in situ LIT for GSL and Baker Lake collected by the Ice Thickness Program Collection, which is available at (https://www.canada.ca/en/services/environment/weather/other-services.html). The data set contains weekly in situ snow and ice thickness measured with drilled holes. The sampling position of GSL is near Yellow Knife (62.4 °N, 114.3 °W) while that of Baker Lake is at 64.3 °N, 96.0 °W. Data records for GSL and Baker Lake have been updated to 2016 and 2020, respectively. To validate the derived altimetric water levels, we obtained daily gauge water levels for GBL, GSL, Athabasca Lake, and Winnipeg Lake collected by the Water Survey of Canada, available at (https://wateroffice.ec.gc.ca/index_e.html). Gauge station names, station codes, locations, and record time span for different lakes are listed in Table 1. The in situ water levels were measured with pressure sensors and therefore represent the free water surface (Yang et al., 2021). Given that in situ and altimetric water levels are based on different datums, we removed the systematic bias between them before making any comparison. The systematic bias is defined as the mean difference between in situ water level time series and altimetric water level time series.

https://doi.org/10.5194/tc-2022-132
Preprint. Discussion started: 26 July 2022

Table 1 In situ lake water level gauging stations used in this study

Lake Name	Station ID	Location	Available records time
Great Bear Lake	10JE002	66°35'59" N 117°37'09" W	1984/7/10–2018/12/31
Great Slave Lake	07OB001	62°26'29" N 114°20'59" W	1934/1/31–2018/12/31
Winnipeg Lake	05SG001	53°11'28" N 99°12'43" W	1953/6/24–2020/12/31
Athabasca Lake	07MC003	59°23'04" N 108°53'34" W	1956/2/25–2020/12/31

We also used modelled LIT to provide cross-validation for lakes without in situ LIT measurements. The modelled LIT data were based on a one dimensional remote sensing lake ice model developed by Li et al. (2022). The modelled LIT is online available at https://doi.org/10.5281/zenodo.5528542.

185

3 Method

A workflow of the methods to retrieve LIT and LSH is illustrated in Fig. 2. Ku-band backscattering coefficients of Jason-1/2/3 were first extracted to classify the type of the observation, i.e., the open water period and the ice-covered period. The LIT would first be estimated based on double-peak waveforms to be illustrated in Sect. 3.1. Then the initial LIT results were used
190 to derive a regression model with Ku-band backscattering coefficients of Jason-1/2/3 to transform backscattering coefficients into LIT to be explained in Sect. 3.2. Subsequently, the LITs based on waveforms and backscattering coefficients were merged and validated/cross-validated against in situ LIT/modelled LIT.

LSH estimation is based on threshold retracking methods to be detailed in Sect. 3.3. For the double-peak waveform in the ice-covered period, only the first subwavefrom is used to retrieve LSH, which is similar to what Yang et al. (2021) have done.
195 Here we used different thresholds (0.1 and 0.5) to generate two LSH time series (LSH_01 and LSH_05 in Fig. 2), because they have different performance in open water and ice-covered periods, i.e., the time series derived from a 0.1 threshold could better reveal the LSH for the ice-covered period, whereas that derived from a 0.5 threshold could better represent the LSH for the open water period. The systematic bias between the two time series based on the 0.1 and 0.5 thresholds during the open water period was removed to merge them into the final LSH time series that were validated with in situ water levels.

https://doi.org/10.5194/tc-2022-132
Preprint. Discussion started: 26 July 2022

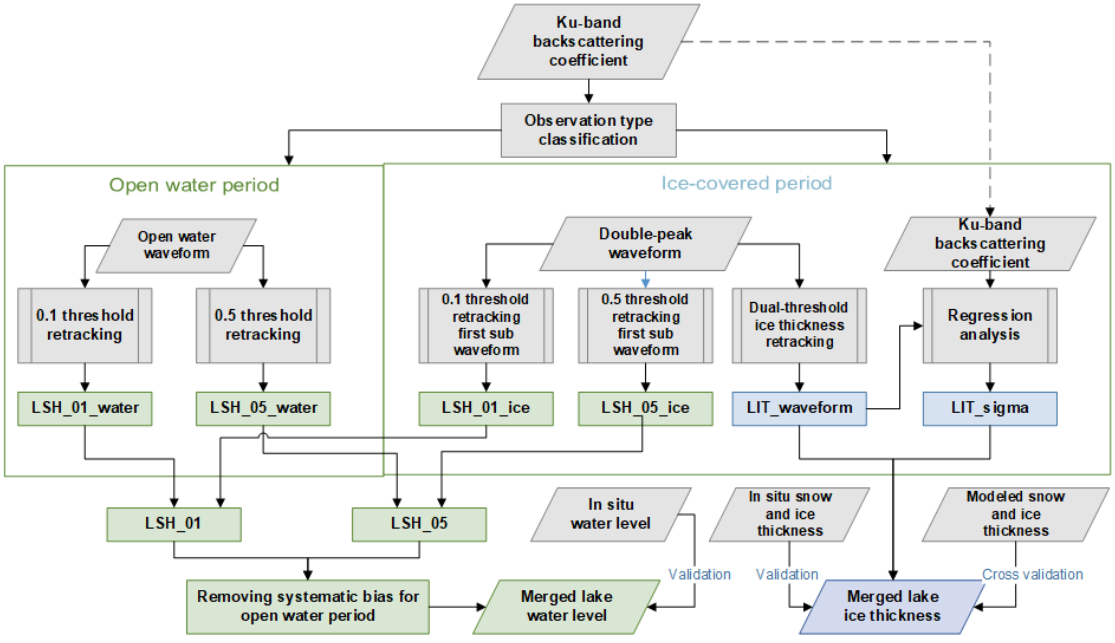

Figure 2: Workflow of this study. Procedures/intermediate data associated with LSH estimation are marked with green. Procedures/intermediate data associated with LIT estimation are marked with blue. LSH_01_water denotes that this intermediate data are lake surface height derived with a 0.1 threshold during the open water period. LSH_01_ice denotes the same meaning but for the ice-covered period. LSH_01 denotes the time series containing all LSHs derived with a 0.1 threshold. Similarly, LSH_05_water, LSH_05_ice, and LSH_05 denote LSHs for different periods derived with a 0.5 threshold. LIT_waveform denotes the LIT derived from double-peak waveforms. LIT_sigma denotes LIT derived from backscattering coefficients.

3.1 LIT retrieval with satellite altimetry waveforms

LIT estimation based on Jason-1/2/3 waveforms was developed by Li et al. (2022). Here we provide the basic concepts and steps of this method and some comparisons with previous studies. Altimetry radar waveforms represent the returned radar wave power as a function of time. When the lake surface is covered with ice and snow, the radar pulse can be backscattered from the air-snow interface, the snow-ice interface, or the ice-water interface. The coupling of signals backscattered from different interfaces could result in the double-peak waveforms. The second peak of the waveform, often highest, is related to the signal from the ice-water interface. However, the source of the first peak is still not clear. The time lag between the two peaks is the time radar pulse transfers between the two interfaces and can be used to calculate the thickness of the medium. Beckers et al. (2017) tested the first peak and the highest peak of CryoSat-2 waveforms to estimate the LIT. The peak associated with the ice-water interface can be easily recognized for beam-limited altimeters such as CryoSat-2, because the beam-limited waveforms have steep trailing edges. Nonetheless, for pulse-limited altimeters with a mild and noisy trailing edge, multiple peaks in the trailing edge are not uncommon, as shown in Fig. 3 (a), making it difficult to choose the correct peak associated

https://doi.org/10.5194/tc-2022-132
Preprint. Discussion started: 26 July 2022

with the ice-water interface. In addition, LITs derived using wave peaks are discrete because the time difference between different peaks is multiple integers of a bin width (3.125 ns for Jason-1/2/3). Therefore, Li et al. (2022) developed a dual-threshold retracking algorithm to estimate the LIT with Jason-1/2/3 waveforms.

Procedures of the dual-threshold retracking method are as follows.

(1) Find the inflection point T on the leading edge of the waveform. If the inflection point appears near the middle of the leading edge, it indicates that there could be two peaks on the leading edge representing the snow/ice surface and ice bottom. If the inflection point appears close to the top of the leading edge, it suggests that there is only one peak on the leading edge and the waveform will be discarded. Assume that the waveform is comprised of P_1, P_2 ... P_N. The wave power difference for adjacent bins can be calculated as $D_i = P_{i+1}$-P_i. S is the STD of D_1, D_2 … D_{N-1}. The first bin of the leading edge is defined as the G0, which satisfies $D_{G0} > 0.2\times S$. Then [G0, G0+15] is defined as the search window. The inflection point T in the search window satisfies $D_T < D_{T-1}$. Subsequently, find the maximum wave power P_M in the search window. If $P_T > 0.9P_M$, discard the waveform, because the inflection point appears near the top of the leading edge.

(2) The first subwaveform associated with the snow/ice surface is defined as [P_{G0}, … P_{T+1}], while the second subwaveform associated with the ice bottom is defined as [P_T, … P_M]. Then, two thresholds (Th_1 and Th_2) can be calculated to determine the two tracking points for the snow/ice surface and ice bottom. Here we used a 0.5 threshold to calculate Th_1 and Th_2, as shown by Equations (1–2). The two tracking points ($T1$ and $T2$) can be calculated with Equations (3–4).

$$Th_1 = 0.5 \times (P_{G0} + P_{T+1}) \quad (1)$$

$$Th_2 = 0.5 \times (P_T + P_M) \quad (2)$$

$$T1 = x + \frac{Th_1 - P_x}{P_{x+1} - P_x}, where\ P_x < Th_1, P_{x+1} > Th_1 \quad (3)$$

$$T2 = y + \frac{Th_2 - P_y}{P_{y+1} - P_y}, where\ P_y < Th_2, P_{y+1} > Th_2 \quad (4)$$

The ice thickness can be calculated as $LIT = 0.5\times(T2\text{-}T1)\times c_i\times 3.125\times 10^{-9}$, where c is the speed of microwave in ice. After acquiring LITs for all footprints for each cycle, the median LIT of each cycle will be used to form the LIT time series.

https://doi.org/10.5194/tc-2022-132
Preprint. Discussion started: 26 July 2022

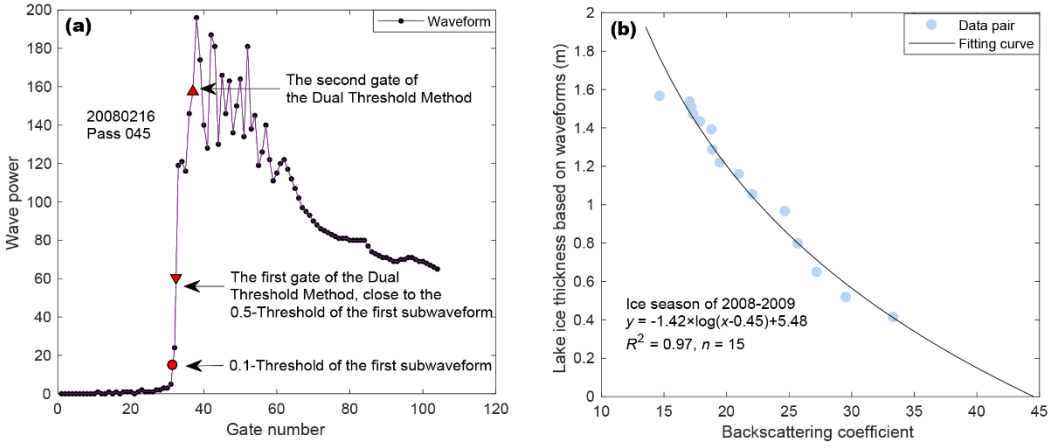

Figure 3: Mechanisms of LIT estimation based on waveforms and backscattering coefficients. (a) a Jason-2 waveform obtained from ice-covered GSL. Red triangles indicate retracking points derived from the dual-threshold retracking algorithm, which can be used to estimate LIT. The red circle represents the retracking point of the first subwaveform with a 0.1 threshold retracker, which can be used to derive LSH. (b) Scatterplot of backscattering coefficients and LIT derived from the dual-threshold retracking algorithm through the ice season of 2008–2009 for GSL. Backscattering coefficients can be transformed into LIT with the derived regression model.

3.2 LIT retrieval with satellite altimetry backscattering coefficients

Evolution in backscattering coefficients during ice seasons is complicated and very different between satellite altimetry and SAR images. For open water, altimetric backscattering coefficients are relatively low, ranging from 10–20 dB for different cycles. For the same cycle, the spatial variation of altimetric backscattering coefficients on the open water is quite small (< 1 dB), as shown by the red curve in Fig. 4(b). Overall, there are four stages of variations in backscattering coefficients with ice evolution during ice seasons (dashed line boxes in Fig. 4(a)). Stage I refers to the period when the lake starts to freeze and be covered by skim ice. During this stage, the altimetric backscattering coefficients soar to a high value in a year (e.g., the first dashed line box in Fig. 4(a)), which could be attributed to the quasi-specular reflecting effect of the smoothed lake surface. Meanwhile, the spatial variation of the altimetric backscattering coefficients becomes relatively large (generally > 2 dB), as shown by the blue curve in Fig. 4(c).

https://doi.org/10.5194/tc-2022-132
Preprint. Discussion started: 26 July 2022

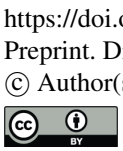

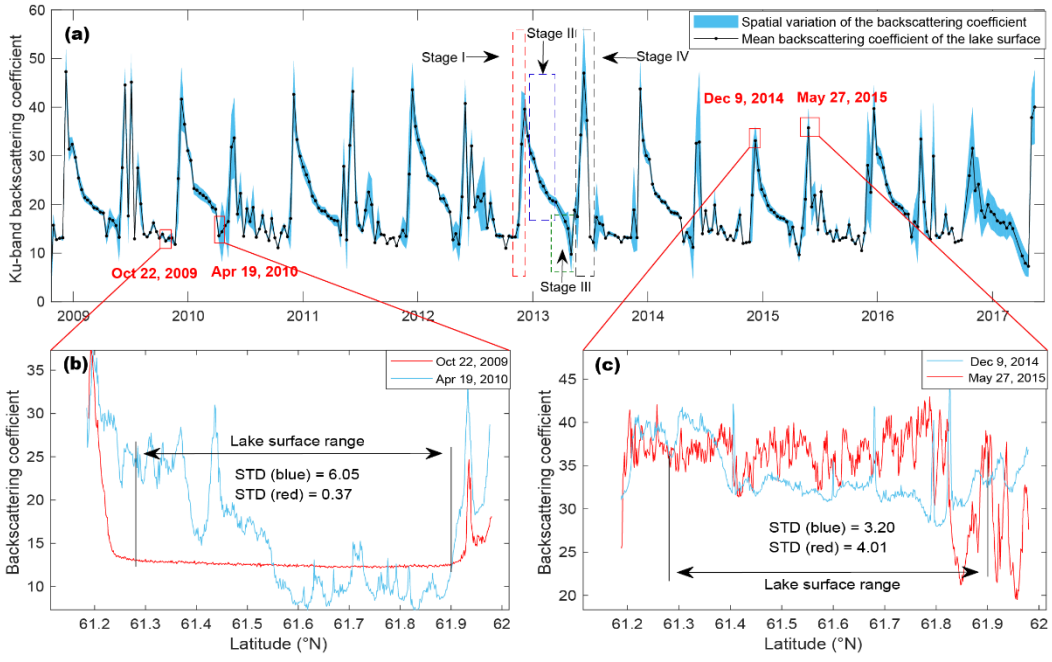

Figure 4: Temporal and spatial variations of Jason-2 Ku-band backscattering coefficients on GSL. (a) Time series of mean backscattering coefficients for each cycle during 2009–2017. Blue shading areas denote the STD of backscattering coefficients for each cycle. (b) and (c) are distributions of the backscattering coefficients along with latitudes for specific cycles/dates (including Oct 22, 2009 and Apr 19, 2010 in (b), and Dec 09, 2014 and May 27, 2015 in (b)). Lake surface latitudinal ranges are marked with double-arrows in (b) and (c).

In comparison, backscattering coefficients derived from SAR images experience high and low values due to wind-induced lake surface roughness for open water periods (Horstmann et al., 2003; Horstmann et al., 2000), but decrease rapidly when the lake starts to freeze. A possible reason why the altimetric backscattering coefficients deviate from those based on SAR images is that altimetry data are nadir-looking observations while most pixels in SAR images are side-looking observations. Consequently, the incident direction is collinear (noncollinear) with the reflection direction for satellite altimetry (SAR images). Therefore, the backscattered energy increases (decreases) by the quasi-specular reflector for satellite altimeters (SAR images). In the following context, the term "backscattering coefficients" refers to altimetry-based backscattering coefficients.

During stage II, with the increase in LIT, the backscattering coefficients start to decrease steadily until the melting starts (e.g., the second dashed line box in Fig.4(a)). The decrease in backscattering coefficients could be attributed to the increased absorption and volume scattering associated with the increased LIT. During stage III when the melting begins, there will be an abrupt decrease in backscattering coefficients (e.g., the third dashed line box in Fig. 4(a)), which is caused partially by ice metamorphism (formation of dendroidal air channels just below the ice surface and early stages of needle ice formation)

https://doi.org/10.5194/tc-2022-132
Preprint. Discussion started: 26 July 2022

(Kouraev et al., 2015). As shown by the blue curve in Fig. 4(b), the backscattering coefficients are very low (e.g., < 10 dB) and noisy over the melting lake surface. The STD of backscattering coefficients for the melting period is much larger than that for the open water period. Based on this phenomenon, we set a criterion (the mean backscattering coefficients < 15 dB and STD > 1.5 dB) to filter out the abrupt decrease in backscattering coefficients when the melting starts, because these low values would lead to unrealistic large LIT estimates.

During stage IV, as the LIT continues to decrease with the melting process, backscattering coefficients start to increase to a high value once again, because of the decrease in absorption and volume scattering effect. Eventually, once the ice completely melts, the backscattering coefficients drop to a level of the open water surface (e.g., the fourth dashed line box in Fig. 4(a)). Therefore, the highest peak in the freezing period and the highest peak in the melting period were chosen to characterize the ice-on and ice-off dates, which classifies the observations into either open water observations or ice-covered observations as suggested by Zakharova et al. (2021).

Based on the variability in backscattering coefficients during the ice seasons, Zakharova et al. (2021) assumed the decrease in backscatter between two consecutive observations to be proportional to the gain in ice thickness and derived a regression model between the cumulative backscatter difference and the in situ river ice thickness on the Lower Ob River. The regression model has the form of $H_i = a \times \mathrm{CumSum}(\mathrm{d}Sig/\mathrm{d}t)^b$, where H_i is the ice thickness, $\mathrm{CumSum}(\mathrm{d}Sig/\mathrm{d}t)$ is the cumulative backscatter difference, and a and b are model parameters calibrated against in situ ice thickness. For simplicity, this model is referred to as the power function model in the following context. The power function model does not consider the physical process associated with ice growth and is dependent on in situ measurements, which limits a wider application of the method. In addition, we found that the performance of LIT estimation using only one regression model with one set of model parameters can be fairly unstable from year to year and from lake to lake, partially because the initial ice and snow conditions can be very different for each winter and each lake, which is also mentioned by Zakharova et al. (2021).

We developed a new regression model considering the physical processes and applied this model to relate backscattering coefficients with LITs derived from waveforms for each lake and during each winter. Therefore, we can circumvent the problems caused by the difference in initial ice and snow conditions. Meanwhile, we can derive LITs based on backscattering coefficients without in situ ice thickness measurements. Because our model has a logarithmic form (equation (10)), it is referred to as the logarithmic model. As shown in Sect. 4.1, the logarithmic model can better represent the LIT compared with the power function model for lakes with thick ice (e.g., > 1 m) and rapid ice accumulation rates.

https://doi.org/10.5194/tc-2022-132
Preprint. Discussion started: 26 July 2022

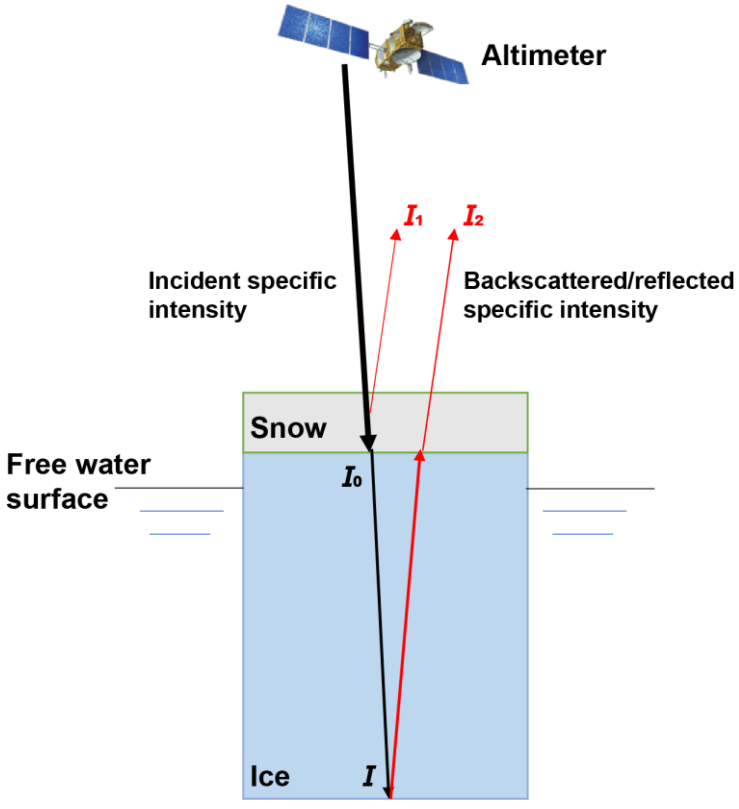

Figure 5: A schematic diagram of radar altimetry specific intensity backscattered/reflected from ice-covered lakes. Black arrows denote the incident specific intensity. Red arrows denote backscattered or reflected specific intensity. I0 denotes the transmitted microwave intensity just below the snow-ice interface. I denotes the transmitted microwave intensity that has just reached the ice-water interface. I1 is the backscattered/reflected intensity from the upper surface (snow surface or the snow-ice interface). I2 is the backscattered/reflected intensity from the ice-water interface. Note that at the nadir the incident angle is small and the backscattered/reflected pulse is approximately colinear with the incident radar pulse.

Theoretically, radar pulse would be backscattered from multiple snow and ice layers, given that different snow/ice layers have different density and temperatures that could influence the backscattering process. The backscattered intensity is a function of the distance, direction, and time that requires detailed modelling, as was done by Larue et al. (2021). To provide a straightforward derivation of the regression model we developed, here we focus on the backscattered intensity of the nadir and assume the radar pulse to be backscattered mostly from two interfaces, i.e., the lower one is the ice-water interface and the upper one could be either the air-snow interface or the snow-ice interface. The backscattered intensity from the upper interface does not change with the LIT. Here we approximate it with a constant I_1 (Fig. 5). The backscattered intensity from the ice-water interface is I_2, which is related to the snow and ice thickness. The total backscattered intensity I_b can be written as Equation (5):

https://doi.org/10.5194/tc-2022-132
Preprint. Discussion started: 26 July 2022

$$I_b = I_1 + I_2 \quad (5)$$

At stage II, backscattering coefficients decrease with the increase in LIT, which could be caused by the increased absorption and volume scattering. Here we approximate the extinction of microwave intensity in snow and ice with an exponential equation as Equation (6):

$$I = I_0 \times e^{-kH_i} \quad (6)$$

where I denotes the transmitted microwave intensity that has just reached the bottom of lake ice, I_0 denotes the transmitted microwave intensity just below the ice surface (assumed to be a constant), k is an effective extinction coefficient, and H_i denotes the thickness of snow and ice.

The backscattered intensity from the ice-water interface I_2 is proportional to I, and it will transmit through the ice and snow again, which can be written as Equation (7), where r is a parameter related to the characteristics of different interfaces (air-snow, snow-ice, and ice-water), such as roughness and relative permittivity.

$$I_2 = r \times I \times e^{-kH_i} \quad (7)$$

Eventually, the total microwave intensity backscattered from the ice-covered lake surface can be approximated by Equation (8). The backscattering coefficient should be proportional to the backscattered intensity I_b. Therefore, we suggest using Equation (9) to relate backscattering coefficients with LIT:

$$I_b = I_1 + I_2 = I_1 + r \times I \times e^{-kH_i} = I_1 + r \times I_0 \times e^{-2kH_i} \quad (8)$$

$$\sigma_0 = A + B \times e^{-KH_i} \quad (9)$$

where σ_0 is the backscattering coefficient, A, B, and K are model parameters to be calibrated. The following strategy can be used to determine the parameters in an efficient way. Parameter A generally ranges from 0 to 20 dB and is not very sensitive. Therefore, discrete values can be assigned to A directly, such as 0, 1, …, 20. Then for each assigned parameter A, transforming Equation (9) into Equation (10) results in the logarithmic regression model:

$$H_i = -\frac{1}{K} \times \ln(\sigma_0 - A) + C, C = \frac{\ln(B)}{K} \quad (10)$$

where parameters K and C in Equation (10) can be determined using linear regression. The residual sum of squares for each set of A, K, and C can be calculated and the parameter group with the lowest residual sum of squares was selected as the final estimates. The calibrated parameters are generally satisfactory as shown in Fig. 3 (b). It is possible that the regression model yields negative LIT at the beginning of the ice seasons because the initial backscattering coefficient exceeds the range of data used in the regression. If that is the case, Equation (9) can be adjusted as Equation (11) to ensure that the initial LIT is non-negative, where σ_{max} is the maximum backscattering coefficient during that ice season.

$$\sigma_0 = A + \sigma_{max} \times e^{-KH_i} \quad (11)$$

https://doi.org/10.5194/tc-2022-132
Preprint. Discussion started: 26 July 2022

3.3 Water level estimation for ice-covered lakes

Yang et al. (2021) developed a straightforward method to retrieve water levels for ice-covered lakes using T/P ad Jason-1/2/3 data. The basic concept of their method is to extract the first subwaveform from the double-peak waveform, and apply the 0.1 threshold retracking algorithm to the first subwaveform. By comparison with in situ water levels, lake ice thickness, and snow depth, Yang et al. (2021) suggested that the first subwaveform retracked with a 0.1 threshold (e.g., the red circle in Fig. 3(a)) is associated with the snow-ice interface and can be used as a good approximation to the free water surface. We noticed that in the dual-threshold retracking algorithm (Li et al., 2022), the first tracking gate (e.g., the first red triangle in Fig. 3(a)) is very close to the 0.5 threshold tracking point of the first subwaveform. By comparing the altimetric LIT with in situ LIT and snow depth, we found that the altimetric LIT is close to the total thickness of ice and snow for most cases, meaning that the first tracking gate is likely associated with the snow surface. Consequently, it becomes a paradox whether the first subwaveform represents signals from the snow surface or the snow-ice interface.

In addition, for a given waveform as shown in Fig. 3 (a), the 0.1 threshold tracking gate (red circle) should be ahead of the 0.5 tracking point (the first red triangle), meaning that the associated surface height of the 0.1 threshold should be higher than that of the 0.5 threshold. But based on the mentioned two studies, the 0.1 threshold is related to the snow-ice interface while the 0.5 threshold is related to the snow surface. The inconsistency between the two studies causes ambiguity in determining the interface associated with the first subwaveform, thereby reducing the reliability of altimetric LIT and LSH for ice-covered lakes.

Therefore, we investigated the LSH for ice-covered lakes using different thresholds. The 0.1 threshold yields higher LSH than the 0.5 threshold for each waveform, meaning that a systematic bias exists between LSH time series from the 0.1 threshold and from the 0.5 threshold. To remove the systematic biases, we chose LSHs during open water periods as the baseline, because observations obtained during open water periods are more stable and robust. For the open water period, the classic 0.1 and 0.5 threshold methods were directly applied to the waveform separately. During the ice-covered period, the 0.1 and 0.5 threshold methods were applied to the first subwaveform. All LSHs for both ice-covered and open water periods derived with the 0.1 threshold were aggregated into one time series, and all LSHs based on the 0.5 threshold were aggregated into the other. The systematic biases between the two time series during open water periods were removed before comparison.

Results shown in Fig. 6 illustrate that with the systematic bias during the open water period removed, the LSH during ice seasons derived from the 0.5 threshold is higher than that derived from the 0.1 threshold, meaning that the 0.5 threshold may correspond to the snow surface and the 0.1 threshold may correspond to the snow-ice interface. Different choices of thresholds would result in different interfaces. We further discuss causes of this phenomenon in Sect. 5, indicating that conclusions from Yang et al. (2021) and Li et al. (2022) are not contradictory.

When comparing LSHs derived from the 0.1 threshold and the 0.5 threshold, we noticed that the 0.5 threshold-based LSHs have a more robust performance during the open water period, corroborated by previous studies (Davis, 1997). For the ice-

https://doi.org/10.5194/tc-2022-132
Preprint. Discussion started: 26 July 2022

covered period, the 0.1 threshold-based LSHs are very close to the in situ water surface as suggested by Yang et al. (2021). Therefore, we merged the two LSH time series (after removing their systematic bias during open water periods) by reserving the 0.5 threshold-based LSHs during the open water period and 0.1 threshold-based LSHs for the ice-covered period to improve the overall performance of water level estimation.

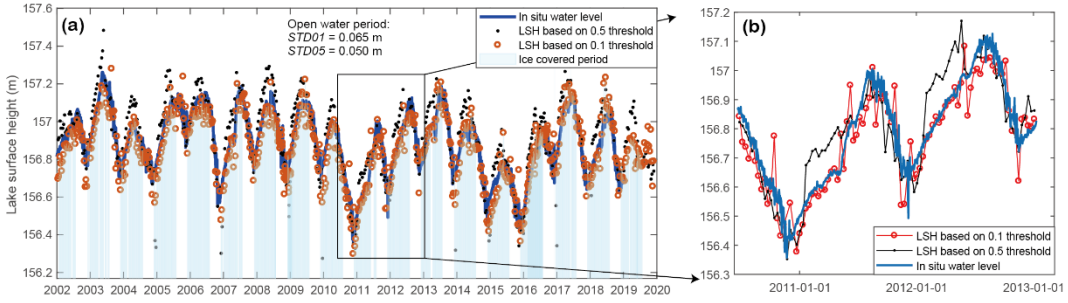

Figure 6: Comparison between LSH estimates using different thresholds in GSL. (a) shows time series for altimetric LSHs based on different thresholds and in situ water levels. (b) is an enlarged view for the LSH time series during 2011–2013. The blue curve denotes in situ water levels, red dots denote LSHs based on a 0.1 threshold, black dots denote LSHs based on a 0.5 threshold, and light blue shading areas denote ice-covered seasons.

4 Results

4.1 Performance of the logarithmic regression model

To evaluate the performance of the logarithmic model we proposed (equation (10)) to convert backscattering coefficients into LIT, we compared it with the power function model used by Zakharova et al. (2021). To evaluate the feasibility of both models, we directly used in situ LIT in Baker Lake instead of waveform-based LIT to generate model parameters, which could represent the best performance of both models ideally. In addition, Zakharova et al. (2021) used parameters derived from training data sets and applied to all ice-covered seasons. Here we derived separate parameters for each ice-covered season for both models due to the large variability of optimal parameter sets in different ice-covered seasons.

As illustrated in Sect. 3.2, the power function model assumes the LIT to be a power function of the accumulated backscattering difference. The LIT naturally starts from zero on the freeze-up date detected by Jason-1/2/3, because the accumulated backscattering difference is zero at the beginning. It has been shown that the power function model is effective in estimating river ice thickness thinner than 1 m. But it is not clear if it is suitable for thicker ice conditions, e.g., in Baker Lake.

The maximum LIT in Baker Lake exceeds 2 m and for most time of the frozen season the LIT is over 1 m, which means that the LIT would increase rapidly at the beginning of ice seasons. Therefore, when Jason-1/2/3 first detected the lake ice in their 10-day revisit cycles, the LIT is not zero but could be several decimetres, which is not fully considered in the power function

https://doi.org/10.5194/tc-2022-132
Preprint. Discussion started: 26 July 2022

model. The logarithmic model, however, is compatible with such kind of initial LIT conditions, as shown by Fig. 7. It is obvious that for the power function model, the initial LIT is estimated as zero but in situ measurements could range from 0.2 to 1 m (Fig. 7(a)).

The logarithmic model could well represent the initial LIT and its overall performance (R^2 of 0.90, RMSE of 0.17 m) is better than that of the power function model (R^2 of 0.77, RMSE of 0.25 m) even if the initial LIT data pairs are removed from the power function model (R^2 of 0.78, RMSE of 0.22 m). In addition, underestimation of LIT is more severe in the power function model when the LIT exceeds 1.5 m, suggesting some saturation effects. Therefore, we suggest to use logarithmic models when the LIT exceeds 1 m or the LIT increases rapidly at the beginning of ice seasons.

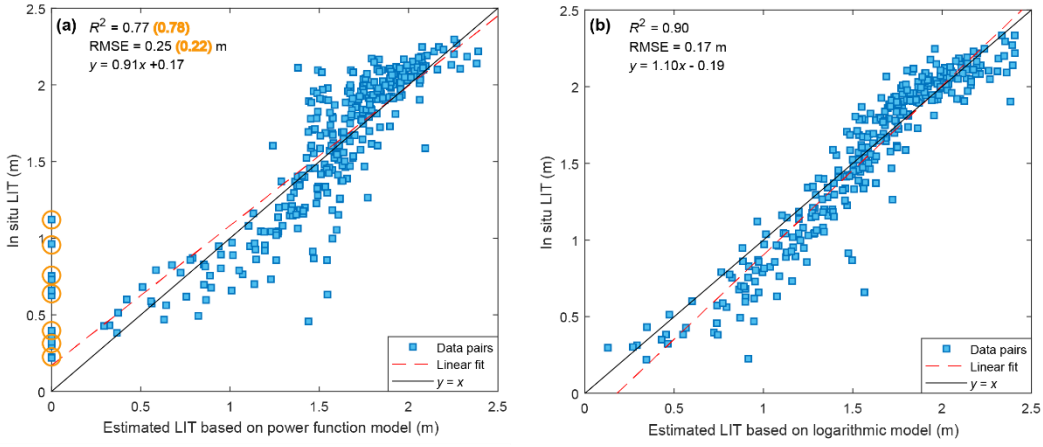

Figure 7: Comparison between in situ and estimated LIT of Baker Lake based on (a) a power function model (Zakharova et al., 2021) and (b) a logarithmic model (this study). For both models, a separate set of parameters were derived for each ice season to best fit the in situ LIT. (a) and (b) are scatterplots of all matched data pairs from 2003 to 2019. Numbers in brackets denote metrics after the removal of outliers marked by yellow circles.

4.2 Altimetry-based LIT estimation

The accuracy of waveform-based LITs has been validated by Li et al. (2022). Therefore, we only validated backscattering coefficient-based LITs against in situ thickness of lake ice and snow here (Fig. 8). The overall performance of the backscattering coefficient-based LIT is close to that based on waveforms. The correlation coefficients (CCs) and RMSEs for Baker Lake and GSL are 0.94 and 0.80, and 0.24 m and 0.17 m, respectively. As suggested by Zakharova et al. (2021), such accuracy is applicable in climate studies but may not meet the need for engineering purposes (e.g., ice roads). The backscattering coefficient-based LITs using our method show metrics slightly lower than that of Zakharova et al. (2021) (RMSE: 0.07–0.18 m). However, the relative errors between the two studies are similar, because the ice thickness on the OB

https://doi.org/10.5194/tc-2022-132
Preprint. Discussion started: 26 July 2022

River is generally smaller than 0.8 m, while the LIT and snow thickness on GSL and Baker Lake could be over 1.5 m and 2 m, respectively. More importantly, our method does not depend on in situ data and can be applied to ungauged lakes without in situ LIT measurements but with altimetric data.

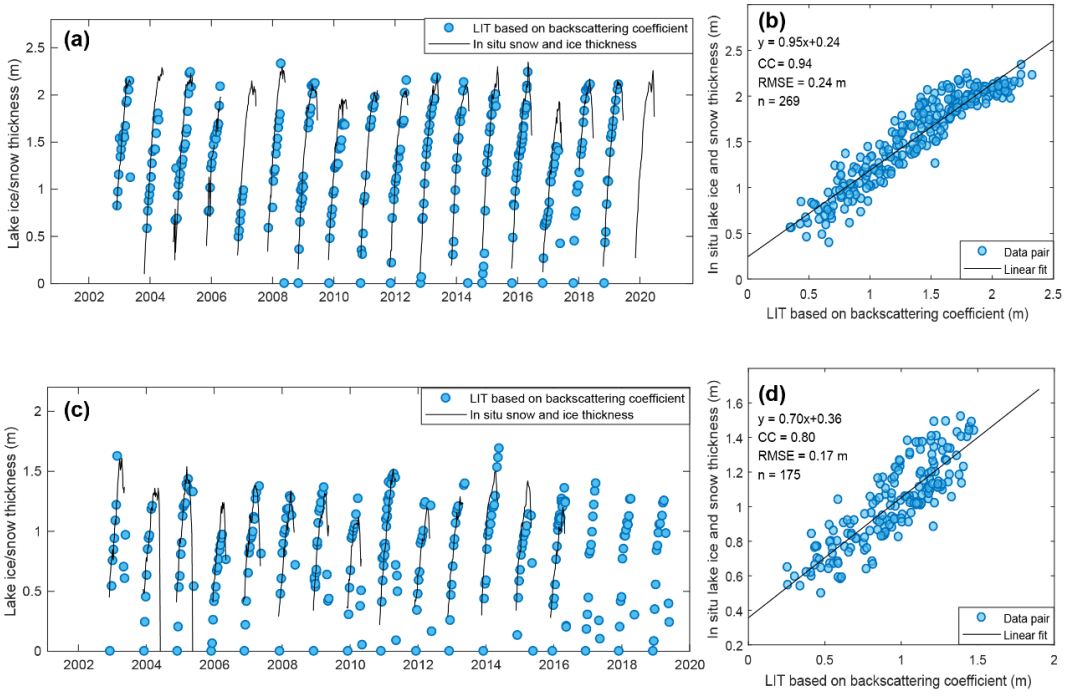

Figure 8: Validation of backscattering coefficient-based LIT against total thickness of ice and snow. (a) and (c) are time series for the backscattering coefficients-based LIT and the in situ lake ice and snow thickness in Baker Lake and GSL. (b) and (d) are scatterplots of backscattering coefficients-based LITs and in situ lake ice and snow thickness in Baker Lake and GSL, respectively.

We also investigated the capability of backscattering coefficient-based LIT to detect thinner ice. First, the LIT time series based on waveforms and backscattering coefficients were merged in a straightforward method: for waveform-based LIT measurements, we reserved those larger than 0.7 m, and for backscattering coefficients-based measurements, we reserved those smaller than 0.7 m. LITs in GSL and Baker lake are relatively large and the ice thickness grows rapidly at the beginning of the ice season, making these lakes not suitable for validating thin ice estimates. Therefore, we made cross-validation between the merged LITs and modelled LITs in lakes with thinner lake ice. i.e., Hulun Lake (117.38 °E 48.97 °N) and Har Lake (93.21 °E 48.05 °N).

Another reason for choosing the two lakes above is that there is little snowfall in these lakes during ice-covered seasons, which can reduce the impact of surface snow because the physical process of surface snow is complicated and could cause large uncertainty in modelled results (Han et al., 2019; Han et al., 2021). The waveform-based LIT in Hulun Lake was not sufficient

https://doi.org/10.5194/tc-2022-132
Preprint. Discussion started: 26 July 2022

to build a regression model (see Sect. 3.2) for each winter before 2014, so we only made cross-validation through 2014–2018. In Har Lake, the cross-validation was made through 2003–2018, as shown in Fig. 9. Overall, the merged altimetric LIT and model results agree well with each other in terms of the coefficient of determination (R^2) of 0.88 for Hulun Lake and 0.79 for Har Lake. But there is a relatively larger discrepancy in Har Lake, which is likely caused by the narrower cross-section of Har Lake and fewer available altimetric footprints.

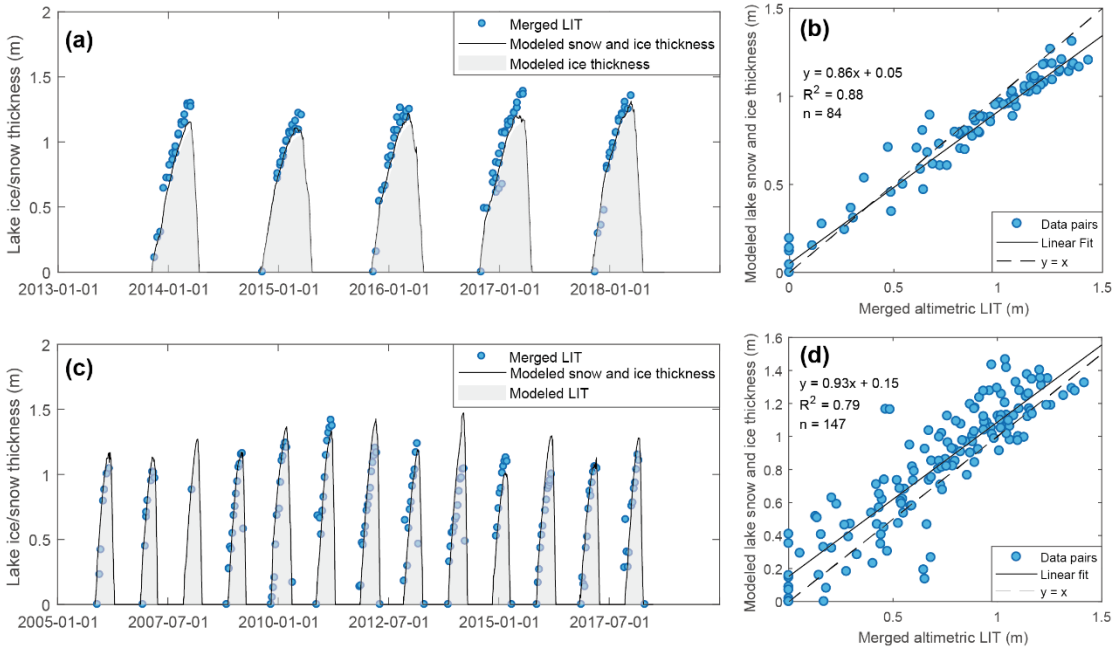

Figure 9: Cross-validation between the merged altimetric LIT (waveforms and backscattering coefficients-based) and modeled lake snow and ice thickness. (a) and (c) are time series for merged altimetric LIT and modeled lake snow and ice for Hulun Lake and Har Lake, where blue dots denote merged altimetric LIT, shading areas denote modeled LIT, and black curves denote modeled lake ice and snow thickness. (b) and (d) are scatterplots for altimetric LIT and modeled lake ice and snow thickness for Hulun Lake and Har Lake, respectively.

4.3 Water level estimation for ice-covered lakes

We derived altimetric LSH time series for four lakes: Athabasca Lake, GBL, GSL, and Winnipeg Lake. Results were validated with in situ water levels using standard deviations of the water level difference (STDs) and RMSEs (Fig. 10). As mentioned in Sect. 3.3, the LSH time series based on both 0.1 and 0.5 thresholds were derived first and then merged into one time series by removing the systematic bias during open water periods. Compared with in situ measurements, the 0.1 threshold-based LSHs outperformed the 0.5 threshold-based LSHs in representing effective water levels during ice-covered periods, while the 0.5 threshold-based LSHs better represent in situ water levels during open water periods (Fig. 6). Therefore, the merged LSH

https://doi.org/10.5194/tc-2022-132
Preprint. Discussion started: 26 July 2022

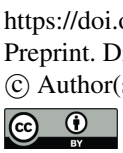

time series should outperform both 0.1 and 0.5 threshold-based LSHs. We did notice an improvement of 1.5–2 cm in metrics (RMSEs and STDs) for each lake. Overall, the metrics of the derived water levels are consistent with those from (Yang et al., 2021) in GSL, GBL, and Athabasca Lake. However, a direct comparison with metrics from (Yang et al., 2021) would be inappropriate, as we used different ground tracks and different gauging stations.

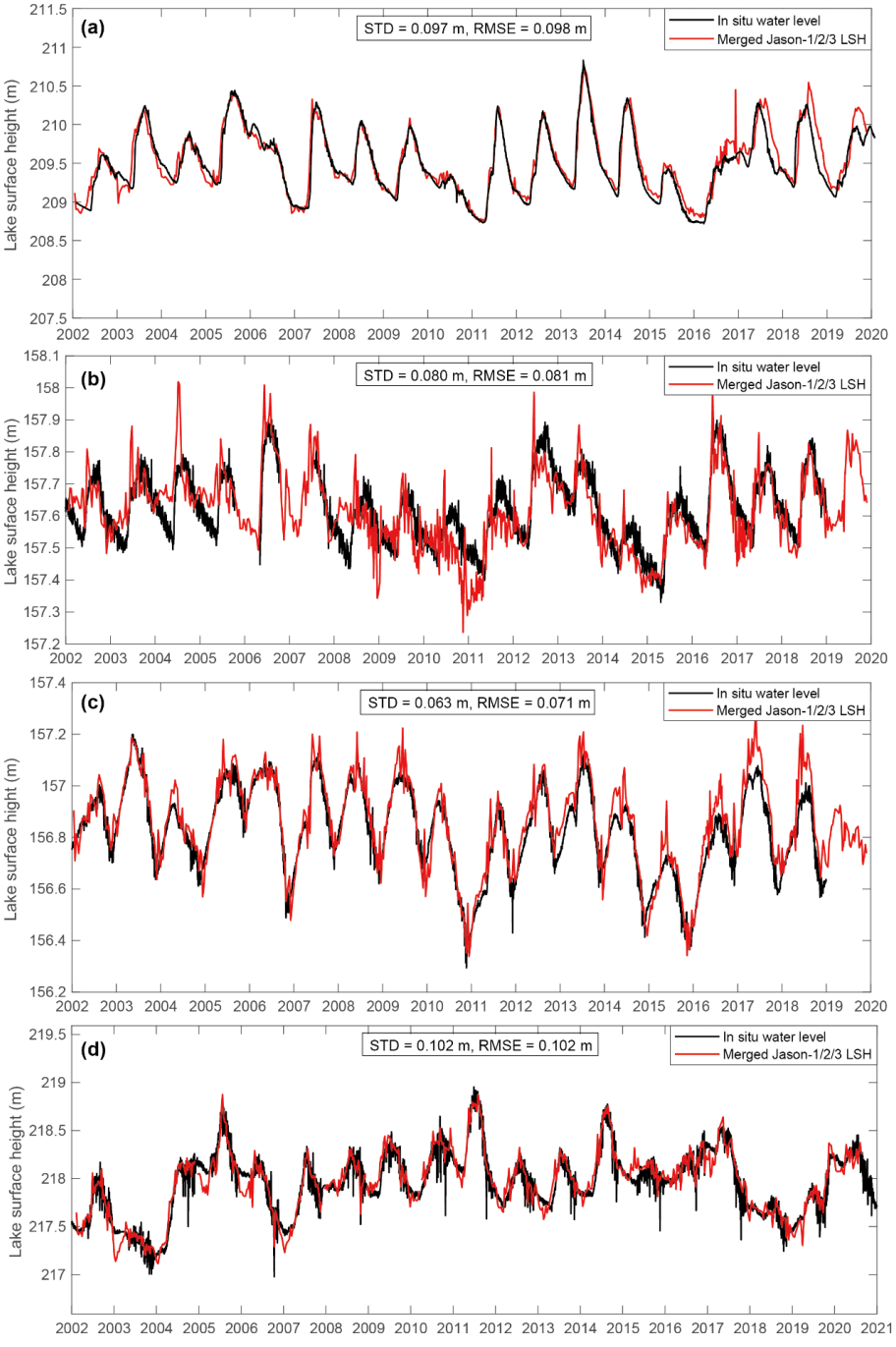

https://doi.org/10.5194/tc-2022-132
Preprint. Discussion started: 26 July 2022

Figure 10: Time series of merged altimetric water levels in Athabasca Lake, GBL, GSL, and Winnipeg Lake. Black curves denote in situ lake water levels and red curves denote merged altimetric LSHs for (a) Athabasca Lake, (b) GBL, (c) GSL, and (d) Winnipeg Lake. Note that there are systematic biases between Jason-1, Jason-2, and Jason-3 data, which were removed by comparing the mean LSHs during the overlapping periods between Jason-1 and Jason-2 (Jul 2008–Jan 2009), and Jason-2 and Jason-3 (Feb 2016–Sep 2016).

Different performance of the merged altimetric LSHs is attributed to different characteristics of variations in lake water level and the duration of lake ice cover. In general, it is more difficult to monitor lakes with larger intra-annual and interannual water level variability. Athabasca Lake and Winnipeg Lake show larger intra-annual variability than GSL and GBL. Consequently, the metrics for Athabasca Lake (STD = 0.097 m) and Winnipeg (STD = 0.102 m) Lake are slightly lower than those from GSL (STD = 0.063 m) and GBL (STD = 0.080 m). In addition, the metrics for GBL are slightly lower than those from GSL, mostly because the ice-covered periods are longer in GBL and the LSHs obtained during ice-covered periods have larger uncertainties than those during open water periods.

5 Discussion

5.1 Conceptual explanation on differences in LSHs derived from different thresholds

Normally a higher threshold of waveform retracking yields a lower LSH, but comparison shown in Fig. 6 indicates that LSHs based on the 0.5 threshold is higher than those based on the 0.1 threshold when the systematic bias during open water periods is removed. Here we provide a conceptual explanation as to why such a phenomenon occurs. As shown in Fig. 11 (a–c), the pulse-limited satellite altimetry sends a microwave pulse with a certain width to the open water surface (with a calm wave surface) and the illuminated area gradually increases to the maximum when the upper bound of the pulse reaches the water surface. Ideally, the largest illuminated area is associated with the peak of the radar waveform (Fig 11 (c)). For threshold retracking methods, a portion of the maximum wave power is used to mark the time when the radar pulse reaches the backscattering surface. For instance, the 0.1 threshold method essentially means that the moment when the echoed radar pulse surpasses a 10% of the peak wave power is chosen to be the time when the radar pulse reaches the lake surface (Fig 11 (a)).

https://doi.org/10.5194/tc-2022-132
Preprint. Discussion started: 26 July 2022

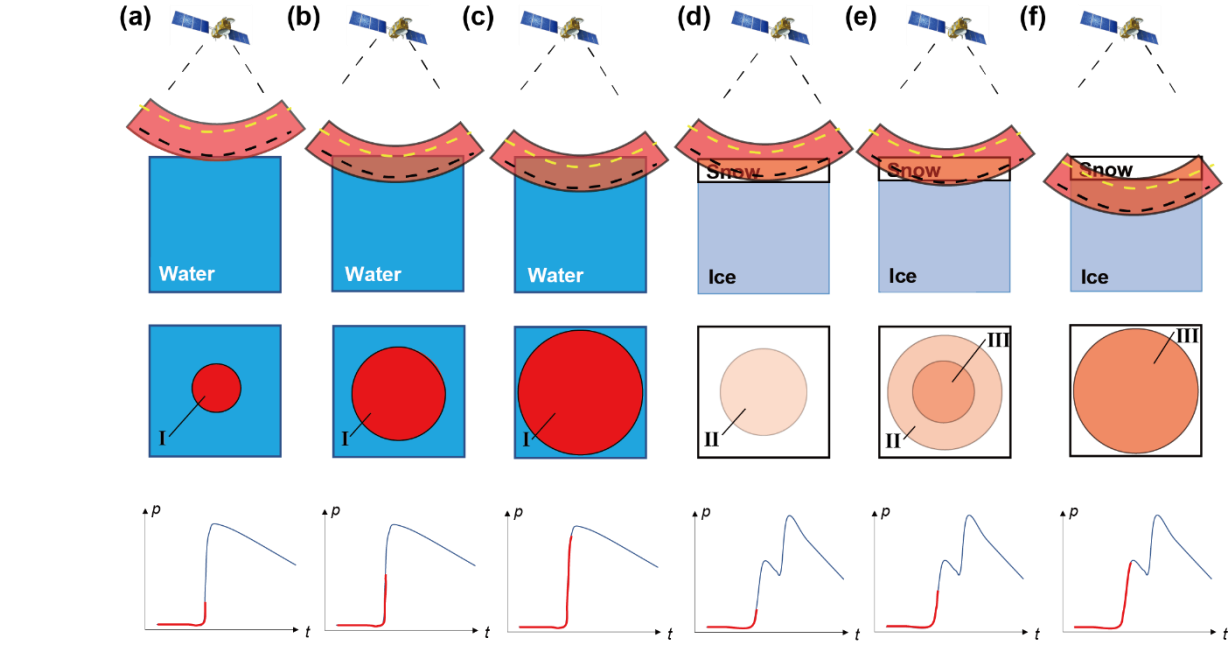

Figure 11: A schematic diagram of pulse-limited radar footprints/illuminated areas and associated waveforms on open water (a–c) and ice-covered (d–f) lakes. The first horizontal panel shows the sideview of the radar pulse and backscattering interfaces. Black and yellow dashed curves denote hypothetic spheres within the radar pulse associated with the 0.1 and 0.5 thresholds, respectively. The second horizontal panel represents the illuminated areas in a vertical view, where circular area I denotes backscattering from the water surface (a–c), circular area II denotes backscattering from snow layers (d and e), circular area III denotes surface backscattering from the snow-ice interface (e and f). The third horizontal panel shows waveforms associated with illuminated areas in the second panel. P represents the returned wave power and t represents the time/gate. The red curve indicates the part of the waveform that has emerged, whereas the blue curve indicates the rest part. Waveforms in (a–c) indicate moments when a 10%, 50%, and 100% of the peak wave power is met, respectively. Waveforms in (d–f) indicate moments when a 10%, 50%, and 100% of the peak in the first subwaveform is met, respectively.

To make the process of the threshold retracking more visible, we assume a sphere within the pulse as shown by the black dashed curve in Fig. 11. The hypothetical sphere is assumed to have a fixed distance/time lag from the lower bound of the radar pulse and we name it the 0.1-shpere for simplicity. The time when the 0.1-sphere reaches the lake surface indicates that the 0.1 threshold is met and an LSH is recorded. The recorded LSH is the absolute height of the radar pulse with respect to the reference ellipsoid or geoid (e.g., for Fig. 11 (a–c), 100 m, 99.5 m, and 99 m). It is also important to know the relative height of the radar pulse with respect to the open water surface, because we used LSHs during the open water period as the baseline to merge LSH time series derived from the 0.1 and 0.5 threshold methods. The 0.1-sphere helps determine the relative height of the radar pulse with respect to the open water surface when the 0.1 threshold method is used. For instance, in Fig. 11 (a–c) relative heights of the radar pulse would be 0, -0.5, and -1 m when the 0.1 threshold method is used. Similarly, we assume a

https://doi.org/10.5194/tc-2022-132
Preprint. Discussion started: 26 July 2022

sphere for the 0.5 threshold method and name it the 0.5-sphere, as shown by the yellow dashed curve in Fig. 11. Relative heights of the radar pulse in Fig. 11 (a–c) would become 0.5, 0, and -0.5 m when the 0.5 threshold is used.

When the lake is covered by snow and ice, the illuminated areas become more complicated (Fig. 11 (d–f)). This is because there are multiple backscattering surfaces and there is also volume backscattering. Consequently, there could be multiple peaks in the waveform. Here, we only focus on the first peak because it is most relevant to either the snow surface or snow-ice interface. Based on previous studies (Atwood et al., 2015; Beckers et al., 2017), we assume the first peak wave power to occur when the upper bound of the pulse reaches the snow-ice interface, as shown in Fig. 11 (f). Then we apply the 0.1 and 0.5 threshold methods to the first peak (Fig. 11 (d–e)). If there is no snow cover, the 0.1 threshold would be met when the 0.1-sphere reaches the ice surface and the 0.5 threshold would be met when the 0.5-sphere reaches the ice surface. However, volume scattering from snow layers contributes to the returned wave power so that the 0.1 threshold is met before the 0.1-sphere reaches the snow-ice interface, albeit close (Fig. 11 (d)). Subsequently, the radar pulse moves a little bit downward and, consequently, the 0.5 threshold is met (Fig. 11 (e)), because the surface backscattering from the snow/ice interface increases significantly. At this moment, the 0.5-sphere (the yellow dashed curve) has just arrived at a height near the snow surface. Therefore, the relative height of the radar pulse in Fig. 11 (d) is close to the snow-ice interface based on the 0.1-sphere, whereas that in Fig. 11 (e) is close to the snow surface based on the 0.5-sphere. Meanwhile, the LSHs recorded in Fig. 11 (d–f) could be 99.6, 99.4, and 98.9 m.

Combining LSHs from the 0.1 threshold (Fig. 11 (a) and (d)), we obtained a hypothetic LSH time series of [100, 99.6] from the 0.1 threshold retracking method. Similarly, combining LSHs from the 0.5 threshold (Fig. 11 (b) and (e)) would result in another LSH time series of [99.5, 99.4] for the 0.5 threshold retracking method. Subsequently, we removed the systematic bias between them during the open water period. For instance, we shifted the 0.1 threshold-based LSHs 0.5 m downward, yielding [99.5, 99.1]. This explains why the 0.1 threshold-based LSHs during ice-covered periods are lower than those from the 0.5 threshold method (Fig. 6). In addition, by comparing the relative heights marked by the 0.1-sphere (Fig.11 (a) and (d)) and 0.5-sphere (Fig.11 (b) and (e)), we found that the 0.1 threshold method could better represent the snow-ice interface, whereas the 0.5 threshold method could correspond to the snow surface during ice seasons.

5.2 Uncertainty and limitations

The main source of uncertainty in LIT estimation is lake-surface snow cover. As a result of the impact of snow cover, the accuracy of remotely-sensed LIT is in general 0.1–0.2 m in current studies. As discussed in Sect. 5.1, lake surface snow could influence radar waveforms as well as backscattering coefficients. On the one hand, physical properties such as density, grain size, and the dielectric constant of lake surface snow that can affect microwave signals have high spatiotemporal variability. On the other hand, in situ measurements of lake surface snow are not sufficient nor accurate enough to support quantification of uncertainty brought by snow cover. For instance, snow depths measured from the lake surface largely deviate from those measured by a meteorological station near Baker Lake (available at https://climate.weather.gc.ca/). The maximum snow depth

https://doi.org/10.5194/tc-2022-132
Preprint. Discussion started: 26 July 2022

recorded from the lake surface is ~20 cm while the maximum snow depth recorded by the meteorological station is generally larger than 50 cm for each ice-covered season. Further investigation is needed to better resolve snow depth and ice thickness for frozen lakes and to better understand the uncertainty of remotely-sensed LIT caused by lake surface snow.

As for the uncertainty of water levels, apart from the impact of snow and altimeter range resolution, the source of uncertainty is associated with remaining systematic biases. Water level time series for ice-covered lakes are based on the connection of observations from Jason-1, Jason-2, and Jason-3 after the removal of systematic biases. To identify systematic biases, mean water levels from different sensors during overlapping periods are compared, which is a technique commonly used. However, it is not clear how much the remaining systematic biases could contribute to the uncertainty of the entire water level series. We estimated that the upper limit of the remaining systematic biases is ~ 5 cm. A detailed description of uncertainty quantification can be found in the Supplementary Information (Supplementary Text 1).

5.3 Implications for future studies

Based on the discussion in Sect. 5.1, different thresholds correspond to different interfaces (e.g., air-snow and snow-ice interfaces) in ice-covered seasons. If the estimation of LSHs with different threshold methods can be further improved, it is possible to discriminate the snow depth from the altimetric LIT. The relationship between backscattering coefficients and the surface snow depth can be further investigated, which could facilitate more robust modelling of lake ice and snow based on backscattering coefficients. It could also facilitate more sophisticated validation of lake ice models containing snow processes.

The method developed here has the potential to be used in early satellite altimetry missions including T/P, ERS-1/2, as well as some follow-on missions such as Jason-CS (Scharroo et al., 2016), extending remotely sensed LIT to three decades and wider spatial coverage. However, it should be investigated whether the developed method is suited for Ka-band altimeters or SAR altimeters such as SARAL/AltiKa, CryoSat-2, and Sentinel-3. This is because the penetration ability of Ka-band microwave and Ku-band microwave in ice and snow could be quite different and the pulse-doppler-limited waveforms (or beam-limited waveforms, e.g., CryoSat-2) are different from pulse-limited waveforms.

6 Conclusion

This study presents an effective method to retrieve LIT based solely on altimetric data (including waveforms and backscattering coefficients), which is applicable to lakes without in situ LIT measurements. We also investigate water level estimation for ice-covered lakes by merging LSH time series derived from different threshold retracking algorithms. Major findings are as follows:

(1) A logarithmic regression model could be more effective in converting backscattering coefficients into LITs than a previously used power function model, in terms of R^2 of 0.90 and RMSE of 0.17 m for the developed logarithmic model.

(2) Validated against in situ measurements and modelled lake ice and snow thickness, the developed altimetric LIT estimation

method combines the advantages from the waveform-based method (physically-based, sensitive to thick ice) and the backscattering coefficient-based method (sensitive to thin ice). The accuracy (or RMSE) of the merged altimetric LIT is ~0.2 m for the study lakes.

(3) Merging LSH time series derived from different threshold retracking algorithms (0.1 and 0.5 thresholds) can improve the performance of water level estimation for the entire study period by 1.5–2 cm, compared to the estimation with single threshold methods in terms of STD or RMSE among the study lakes.

(4) Different threshold retracking algorithms (0.1 and 0.5 thresholds) can represent different backscattering surfaces for ice-covered lakes. Compared to the same baseline (LSH during open water period), the 0.1 threshold could represent the snow-ice interface while the 0.5 threshold could represent the air-snow interface.

Overall, we provide a more robust and adaptive method for remote sensing of LIT and LSH for ice-covered lakes without in situ observations. The differential impact of lake surface snow on different threshold methods and its implications in future research related to altimetric LIT and water level estimation are discussed. This study facilitates a better interpretation of satellite altimetry signals from ice-covered lakes and provides opportunities for a wider application of altimetry data to the cryosphere.

Author Contributions:

Conceptualization, X.L. and D.L.; methodology, X.L. and D.L.; data curation, X.L.; writing-original draft preparation, X.L.; writing-review and editing, D.L., Y.C., T.L., J.L., M.A.H., and M.M.M.

Conflicts of Interest: The authors declare no conflict of interest.

Data and Code Availability Statement:

The data and code presented in this study are available on a reasonable request from the corresponding author.

Acknowledgements

This work was supported by the Major Science and Technology Projects of Inner Mongolia Autonomous Region (2020ZD0009) and National Natural Science Foundation of China (92047301). Reviewers and editors' comments that are useful to improve this study and manuscript are highly appreciated. The authors sincerely thank the Canadian Ice Service for providing in situ lake ice and snow thickness, the Water Survey of Canada for providing the in situ water levels, and the AVISO+ for providing the satellite altimetry data that enabled us to conducte this study.

https://doi.org/10.5194/tc-2022-132
Preprint. Discussion started: 26 July 2022

References

Atwood, D. K., Gunn, G. E., Roussi, C., Wu, J., Duguay, C., and Sarabandi, K.: Microwave backscatter from Arctic lake ice and polarimetric implications, IEEE Trans. Geosci. Remote Sens., 53, 5972-5982, 10.1109/TGRS.2015.2429917, 2015.

Beckers, J. F., Casey, J. A., and Haas, C.: Retrievals of Lake Ice Thickness From Great Slave Lake and Great Bear Lake Using CryoSat-2, IEEE Trans. Geosci. Remote Sens., 55, 3708-3720, 10.1109/TGRS.2017.2677583, 2017.

Cai, Z., Jin, T., Li, C., Ofterdinger, U., Zhang, S., Ding, A., and Li, J.: Is China's fifth-largest inland lake to dry-up? Incorporated hydrological and satellite-based methods for forecasting Hulun lake water levels, Adv. Water Resour., 94, 185-199, 10.1016/j.advwatres.2016.05.010, 2016.

Cheng, B., Mäkynen, M., Similä, M., Rontu, L., and Vihma, T.: Modelling snow and ice thickness in the coastal Kara Sea, Russian Arctic, Ann. Glaciol., 54, 105-113, 10.3189/2013AoG62A180, 2013.

Cooley, S. W., Ryan, J. C., Smith, L. C., Horvat, C., Pearson, B., Dale, B., and Lynch, A. H.: Coldest Canadian Arctic communities face greatest reductions in shorefast sea ice, Nat. Clim. Change., 10, 533-538, 10.1038/s41558-020-0757-5, 2020.

Davis, C. H.: A robust threshold retracking algorithm for measuring ice-sheet surface elevation change from satellite radar altimeters, IEEE Trans. Geosci. Remote Sens., 35, 974-979, 10.1109/36.602540, 1997.

Du, J., Kimball, J. S., Duguay, C., Kim, Y., and Watts, J. D.: Satellite microwave assessment of Northern Hemisphere lake ice phenology from 2002 to 2015, The Cryosphere, 11, 47, 10.5194/tc-11-47-2017, 2017.

Duguay, C. and Lafleur, P.: Determining depth and ice thickness of shallow sub-Arctic lakes using space-borne optical and SAR data, Int. J. Remote Sens., 24, 475-489, 10.1080/01431160304992, 2003.

Duguay, C. R., Flato, G. M., Jeffries, M. O., Menard, P., Morris, K., and Rouse, W. R.: Ice-cover variability on shallow lakes at high latitudes: model simulations and observations, Hydrol. Processes, 17, 3465-3483, 10.1002/hyp.1394, 2003.

Engram, M., Anthony, K. W., Sachs, T., Kohnert, K., Serafimovich, A., Grosse, G., and Meyer, F.: Remote sensing northern lake methane ebullition, Nat. Clim. Change., 10, 511–517, 10.1038/s41558-020-0762-8, 2020.

Han, P. F., Long, D., Han, Z. Y., Du, M. D., Dai, L. Y., and Hao, X. H.: Improved understanding of snowmelt runoff from the headwaters of China's Yangtze River using remotely sensed snow products and hydrological modeling, Remote Sens. Environ., 224, 44-59, 10.1016/j.rse.2019.01.041, 2019.

Han, Z. Y., Long, D., Han, P. F., Huang, Q., Du, M. D., and Hou, A. Z.: An improved modeling of precipitation phase and snow in the Lancang River Basin in Southwest China, Science China-Technological Sciences, 64, 1513-1527, 10.1007/s11431-020-1788-4, 2021.

Horstmann, J., Koch, W., Lehner, S., and Tonboe, R.: Wind retrieval over the ocean using synthetic aperture radar with C-band HH polarization, IEEE Trans. Geosci. Remote Sens., 38, 2122-2131, 10.1109/36.868871, 2000.

Horstmann, J., Schiller, H., Schulz-Stellenfleth, J., and Lehner, S.: Global wind speed retrieval from SAR, IEEE Trans. Geosci. Remote Sens., 41, 2277-2286, 10.1109/tgrs.2003.814658, 2003.

https://doi.org/10.5194/tc-2022-132
Preprint. Discussion started: 26 July 2022

Howell, S. E. L., Brown, L. C., Kang, K.-K., and Duguay, C. R.: Variability in ice phenology on Great Bear Lake and Great Slave Lake, Northwest Territories, Canada, from SeaWinds/QuikSCAT: 2000-2006, Remote Sens. Environ., 113, 816-834, 10.1016/j.rse.2008.12.007, 2009.

Howell, S. E. L., Small, D., Rohner, C., Mahmud, M. S., Yackel, J. J., and Brady, M.: Estimating melt onset over Arctic sea ice from time series multi-sensor Sentinel-1 and RADARSAT-2 backscatter, Remote Sens. Environ., 229, 48-59, 10.1016/j.rse.2019.04.031, 2019.

Howell, S. E. L., Komarov, A. S., Dabboor, M., Montpetit, B., Brady, M., Scharien, R. K., Mahmud, M. S., Nandan, V., Geldsetzer, T., and Yackel, J. J.: Comparing L- and C-band synthetic aperture radar estimates of sea ice motion over different ice regimes, Remote Sens. Environ., 204, 380-391, 10.1016/j.rse.2017.10.017, 2018.

Huang, Q., Li, X. D., Han, P. F., Long, D., Zhao, F. Y., and Hou, A. Z.: Validation and application of water levels derived from Sentinel-3A for the Brahmaputra River, Science China-Technological Sciences, 62, 1760-1772, 10.1007/s11431-019-9535-3, 2019.

Huang, Q., Long, D., Du, M., Zeng, C., Li, X., Hou, A., and Hong, Y.: An improved approach to monitoring Brahmaputra River water levels using retracked altimetry data, Remote Sens. Environ., 211, 112-128, 10.1016/j.rse.2018.04.018, 2018.

Kang, K.-K., Duguay, C. R., Howell, S. E., Derksen, C. P., and Kelly, R. E.: Sensitivity of AMSR-E brightness temperatures to the seasonal evolution of lake ice thickness, IEEE Geosci. Remote Sens. Lett., 7, 751-755, 10.1109/LGRS.2010.2044742, 2010.

Kang, K. K., Duguay, C. R., Lemmetyinen, J., and Gel, Y.: Estimation of ice thickness on large northern lakes from AMSR-E brightness temperature measurements, Remote Sens. Environ., 150, 1-19, 10.1016/j.rse.2014.04.016, 2014.

Knoll, L. B., Sharma, S., Denfeld, B. A., Flaim, G., Hori, Y., Magnuson, J. J., Straile, D., and Weyhenmeyer, G. A.: Consequences of lake and river ice loss on cultural ecosystem services, Limnol. Oceanogr. Lett, 4, 119-131, 10.1002/lol2.10116, 2019.

Kouraev, A. V., Zakharova, E. A., Remy, F., and Suknev, A. Y.: Study of Lake Baikal Ice Cover from Radar Altimetry and In-Situ Observations, Mar. Geod., 38, 477-486, 10.1080/01490419.2015.1008155, 2015.

Kropácek, J., Maussion, F., Chen, F., Hoerz, S., and Hochschild, V.: Analysis of ice phenology of lakes on the Tibetan Plateau from MODIS data, The Cryosphere, 7, 287, 10.5194/tc-7-287-2013, 2013.

Larue, F., Picard, G., Aublanc, J., Arnaud, L., Robledano-Perez, A., Le Meur, E., Favier, V., Jourdain, B., Savarino, J., and Thibaut, P.: Radar altimeter waveform simulations in Antarctica with the Snow Microwave Radiative Transfer Model (SMRT), Remote Sens. Environ., 263, 10.1016/j.rse.2021.112534, 2021.

Li, X., Long, D., Huang, Q., and Zhao, F.: The state and fate of lake ice thickness in the Northern Hemisphere, Sci. Bull., 67, 537-546, 10.1016/j.scib.2021.10.015, 2022.

Li, X., Long, D., Huang, Q., Han, P., Zhao, F., and Wada, Y.: High-temporal-resolution water level and storage change data sets for lakes on the Tibetan Plateau during 2000–2017 using multiple altimetric missions and Landsat-derived lake shoreline positions, Earth Syst. Sci. Data, 11, 1603-1627, 10.5194/essd-11-1603-2019, 2019.

Medeiros, A. S., Friel, C. E., Finkelstein, S. A., and Quinlan, R.: A high resolution multi-proxy record of pronounced recent environmental change at Baker Lake, Nunavut, J. Paleolimnol., 47, 661-676, 10.1007/s10933-012-9589-2, 2012.

Mullan, D., Swindles, G., Patterson, T., Galloway, J., Macumber, A., Falck, H., Crossley, L., Chen, J., and Pisaric, M.: Climate change and the long-term viability of the World's busiest heavy haul ice road, Theor. Appl. Climatol., 129, 1089-1108, 10.1007/s00704-016-1830-x, 2017.

Murfitt, J. and Duguay, C. R.: 50 years of lake ice research from active microwave remote sensing: Progress and prospects, Remote Sens. Environ., 264, 112616, 10.1016/j.rse.2021.112616, 2021.

Murfitt, J. C., Brown, L. C., and Howell, S. E. L.: Estimating lake ice thickness in Central Ontario, PLOS ONE, 13, e0208519, 10.1371/journal.pone.0208519, 2018.

Scharroo, R., Bonekamp, H., Ponsard, C., Parisot, F., von Engeln, A., Tahtadjiev, M., de Vriendt, K., and Montagner, F.: Jason continuity of services: continuing the Jason altimeter data records as Copernicus Sentinel-6, Ocean Sci., 12, 471-479, 10.5194/os-12-471-2016, 2016.

Sharma, S., Blagrave, K., Magnuson, J. J., O'Reilly, C. M., Oliver, S., Batt, R. D., Magee, M. R., Straile, D., Weyhenmeyer, G. A., and Winslow, L.: Widespread loss of lake ice around the Northern Hemisphere in a warming world, Nat. Clim. Change., 9, 227-231, 10.1038/s41558-018-0393-5, 2019.

Sharma, S., Blagrave, K., Watson, S. R., O'Reilly, C. M., Batt, R., Magnuson, J. J., Clemens, T., Denfeld, B. A., Flaim, G., and Grinberga, L.: Increased winter drownings in ice-covered regions with warmer winters, PLOS ONE, 15, e0241222, 2020.

Shu, S., Liu, H., Beck, R. A., Frappart, F., Korhonen, J., Xu, M., Yang, B., Hinkel, K. M., Huang, Y., and Yu, B.: Analysis of Sentinel-3 SAR altimetry waveform retracking algorithms for deriving temporally consistent water levels over ice-covered lakes, Remote Sens. Environ., 239, 111643, 10.1016/j.rse.2020.111643, 2020.

Stewardship, M. W.: State of Lake Winnipeg: 1999 to 2007, Environment Canada and Manitoba Water Stewardship, 2011.

Wang, W., Lee, X., Xiao, W., Liu, S., Schultz, N., Wang, Y., Zhang, M., and Zhao, L.: Global lake evaporation accelerated by changes in surface energy allocation in a warmer climate, Nat. Geosci., 11, 410-414, 10.1038/s41561-018-0114-8, 2018.

Wik, M., Varner, R. K., Anthony, K. W., MacIntyre, S., and Bastviken, D.: Climate-sensitive northern lakes and ponds are critical components of methane release, Nat. Geosci., 9, 99-105, 10.1038/ngeo2578, 2016.

Woolway, R. I., Kraemer, B. M., Lenters, J. D., Merchant, C. J., O'Reilly, C. M., and Sharma, S.: Global lake responses to climate change, Nature Reviews Earth & Environment, 1, 388–403, 10.1038/s43017-020-0067-5, 2020.

Yang, X., Pavelsky, T. M., and Allen, G. H.: The past and future of global river ice, Nature, 577, 69-73, 10.1038/s41586-019-1848-1, 2020.

Yang, Y., Moore, P., Li, Z., and Li, F.: Lake Level Change From Satellite Altimetry Over Seasonally Ice-Covered Lakes in the Mackenzie River Basin, IEEE Trans. Geosci. Remote Sens., 59, 8143-8152, 10.1109/tgrs.2020.3040853, 2021.

Yu, Y. and Rothrock, D.: Thin ice thickness from satellite thermal imagery, J. Geophys. Res. Oceans, 101, 25753-25766, 1996.

https://doi.org/10.5194/tc-2022-132
Preprint. Discussion started: 26 July 2022

Zakharova, E., Agafonova, S., Duguay, C., Frolova, N., and Kouraev, A.: River ice phenology and thickness from satellite altimetry: potential for ice bridge road operation and climate studies, The Cryosphere, 15, 5387-5407, 10.5194/tc-15-5387-2021, 2021.

Zeng, T., Shi, L., Marko, M., Cheng, B., Zou, J., and Zhang, Z.: Sea ice thickness analyses for the Bohai Sea using MODIS thermal infrared imagery, Acta Ocean. Sin., 35, 96-104, 10.1007/s13131-016-0908-8, 2016.

Zhang, G., Ran, Y., Wan, W., Luo, W., Chen, W., Xu, F., and Li, X.: 100 years of lake evolution over the Qinghai–Tibet Plateau, Earth Syst. Sci. Data, 13, 3951-3966, 10.5194/essd-13-3951-2021, 2021.

Zhao, F., Long, D., Li, X., Huang, Q., and Han, P.: Rapid glacier mass loss in the Southeastern Tibetan Plateau since the year 2000 from satellite observations, Remote Sens. Environ., 270, 112853, 10.1016/j.rse.2021.112853, 2022.

Ziyad, J., Goita, K., Magagi, R., Blarel, F., and Frappart, F.: Improving the Estimation of Water Level over Freshwater Ice Cover using Altimetry Satellite Active and Passive Observations, Remote Sensing, 12, 10.3390/rs12060967, 2020.